AIAA JOURNAL
Vol. 46, No. 11, November 2008

Organized Self-Sustained Oscillations of Turbulent Flows over an Open Cavity

Sang Bong Lee,* Woong Kang,* and Hyung Jin Sung†
Korea Advanced Institute of Science and Technology, Daejeon 305-701, Republic of Korea

DOI: 10.2514/1.36860

Proper orthogonal decomposition was employed to turbulent flows over an open cavity to investigate the spatial characteristics of coherent structures responsible for self-sustained oscillations. The distributions of pressure fluctuations were analyzed by using snapshot-based proper orthogonal decomposition. When self-sustained oscillations took place for $Re_D = 12,000$ in the cavity geometry of $L/D = 2$, three pairs of alternative patterns were shown in the first and second modes of pressure fluctuations. By examining both temporal evolutions and spanwise distributions of the first two modes, quasi-two-dimensional vortical formations were shown to be responsible for the self-sustained oscillations. In turbulent cavity flows of $Re_D = 3000$, however, the periodic oscillations were not observed, due to the irregular shedding of three-dimensional vortical structures. For the application of proper orthogonal decomposition analysis to experimental data, the decomposition was employed to the spatial distributions of v-v correlations on the lip line of cavity geometry.

Nomenclature

a_m	=	time-varying coefficient of mth mode
$\mathbf{c}_m$	=	mth eigenvector
c_m	=	ith element of eigenvector $\mathbf{c}_m$
D	=	cavity depth
f, ω	=	frequency of self-sustained oscillations, $\omega = 2\pi f$
K	=	kernel function
L	=	cavity length
L_i	=	streamwise lengths of the development section before the leading edge
L_o	=	streamwise lengths of the development section after the trailing edge
L_Y	=	transverse length of computational domain
L_Z	=	spanwise length of computational domain
M	=	total number of eigenmodes or snapshots
N	=	number of self-sustained oscillation modes
N_i	=	number of grids in each directions
p'	=	pressure fluctuations
q	=	stochastic data
Re_D	=	Reynolds number, $U_\infty D/\nu$
Re_θ	=	Reynolds number, $U_\infty \theta/\nu$
tU_∞/D	=	nondimensionalized time
U_C	=	convection velocity
U_∞	=	freestream velocity
x_i	=	Cartesian coordinate
α_m	=	mth threshold of time-varying coefficient
γ_m, μ_m	=	mth eigenvalue
Δt	=	computational time step
η	=	residual of eigenmode
θ	=	momentum thickness of incoming boundary layer
ν	=	kinematic viscosity
σ_m, ψ_m	=	mth eigenmode
Ω	=	physical domain of stochastic data
$+$	=	wall unit

Received 26 January 2008; accepted for publication 24 June 2008.

*Department of Mechanical Engineering, 373-1 Guseong-dong, Yuseong-gu.

†Corresponding Author, Department of Mechanical Engineering, 373-1 Guseong-dong, Yuseong-gu; hjsung@kaist.ac.kr.

I. Introduction

THE occurrence of self-sustained oscillations has been the most important characteristic in the behaviors of a separated shear layer over an open cavity since Rossiter [1] investigated the influence of cavity dimensions and freestream velocity on resonant tones. To understand the mechanism underlying self-sustained oscillations and elucidate large-scale vortical structures responsible for such oscillations, numerous experimental and numerical studies have been carried out in incompressible flows as well as in compressible flows. As reported in the previous studies of compressible flows [2,3], the mechanism of self-sustained oscillations has been well characterized by extracting large-scale vortical structures from compressible flows over an open cavity.

In incompressible turbulent flows, however, it has not been easy to identify coherent structures responsible for the oscillations due to both incompressibility and turbulence, although self-sustained oscillations have been expected to take place. The absence of acoustic resonance leads to weak oscillation of the separated shear layer and the coherent structures are mixed with the inherent turbulent motions. It may be the main reason why the vortical formation of large-scale structures was carefully shown in instantaneous velocity and vorticity fields rather than a statistical analysis [4]. Instantaneous fields of velocity fluctuations were mainly used in Ashcroft and Zhang [5] to show large-scale vortical structures in a separated shear layer although the organized nature of coherent structures was reflected by the statistical analysis of v correlations. The work of Kang et al. [6], which was the first large-eddy simulation (LES) of high Reynolds number in incompressible turbulent flows over an open cavity, also provided instantaneous isopleths and spanwise-averaged contours of pressure fluctuations to show large-scale vortical structures responsible for the peak frequency of energy spectra. Because the examination of raw data, including instantaneous velocity or vorticity distributions, restricts the structural analysis of a separated shear layer to be instant and qualitative, a statistical analysis such as proper orthogonal decomposition (POD) is necessary to elucidate quantitative characteristics of large-scale vortical structures.

The proper orthogonal decomposition is a basic statistical tool which is a procedure for finding an orthonormal basis set from an ensemble of stochastic data. Since the POD was first introduced in turbulent flows by Lumley [7], the decomposition has been frequently used in analyzing the properties of coherent structures embedded in background turbulent noises and constructing low-dimensional models that exhibit most of the coherent properties. In turbulent channel flows, an one-dimensional POD analysis was carried out to determine the scale and pattern of large-scale structures

that contribute most to the total turbulent kinetic energy [8]. In separated shear flows, Kostas et al. [9] performed the POD analysis on both fluctuating velocity and vorticity fields of a backward-facing step, which was obtained from particle image velocimetry (PIV) measurements. Not only the velocity field but surface pressure was analyzed by using the decomposition to identify large-scale vortical structures that generate the pressure fluctuations on the bottom surface of a backward-facing step [10]. The POD was also employed to 2-D compressible laminar flows over a rectangular cavity to obtain a low-order dynamic model for the oscillating behaviors of a separated shear layer [6]. Pastur et al. [11] applied the decomposition to 2-D snapshots of incompressible laminar flows to expose the spatial coherent structures that give rise to self-sustained oscillations. By examining the temporal evolutions of dominant eigenmodes, the first two eigenmodes were ascertained to be responsible for the peak frequency of power spectral distribution. The 2-D POD was extended to a 3-D decomposition in Podvin et al. [12]. From the temporal spectra of time-varying coefficients, it was shown that the 3-D POD was more adequate for capturing the oscillating behaviors of the separated shear layer than the 2-D POD. Although the 2-D POD provided a mixture of "shear-layer" and "cavity" modes due to the loss of three-dimensionality, the 2-D decomposition was still useful for distinguishing large-scale coherent structures from the inherent fluctuations of the separated shear layer.

Despite the attractiveness of POD analysis for identifying large-scale coherent structures, the application of POD to incompressible turbulent flows over an open cavity has received little attention because large-scale vortical structures are difficult to identify due to the weak coherence of large-scale structures in the absence of acoustic resonance. The objectives of the present study are to 1) identify large-scale vortical structures responsible for hydrodynamic oscillations by employing the POD to the pressure fluctuations of incompressible turbulent flows over an open cavity; 2) obtain the vector fields of velocity fluctuations corresponding to the dominant eigenmodes of pressure fluctuations with the concept of conditional averaging; 3) elucidate the quantitative characteristics of large-scale vortical structures by comparing the oscillating behaviors of a separated shear layer with those of a nonoscillating system. To achieve these, numerical data of Kang et al. [6] are analyzed by using 2-D POD. Furthermore, because the spatial distributions of pressure fluctuations are not available in the experimental application of the decomposition, the distributions of v-v correlations are used in the POD analysis to represent the oscillating behaviors of a separated shear layer over an open cavity.

II. Numerical and Experimental Procedures

For an incompressible flow, the nondimensional governing equations are

$$\frac{\partial u_i}{\partial t} + \frac{\partial u_i u_j}{\partial x_j} = -\frac{\partial p}{\partial x_i} + \frac{1}{Re_D}\frac{\partial^2 u_i}{\partial x_j^2}, \qquad i = 1, 2, 3 \tag{1}$$

$$\frac{\partial u_i}{\partial x_i} = 0 \tag{2}$$

where x_i are the Cartesian coordinates and u_i are the corresponding velocity components. The freestream velocity U_∞ and the cavity depth D are used for nondimensionalization. The Reynolds number is defined as $Re_D = U_\infty D/\nu$, where ν is the kinematic viscosity. The governing equations are integrated in time using the fully implicit decoupling method proposed by Kim et al. [13]. All terms are advanced in time with the Crank–Nicolson method, and are resolved with the second-order central difference scheme in space. Based on a block LU decomposition, both velocity-pressure decoupling and additional decoupling of the intermediate velocity components are achieved in conjunction with the approximate factorization. The multigrid method is applied to obtain the solution of the pressure Poisson equation in a T-shaped domain.

A schematic of the computational domain is shown in Fig. 1. For all of the present simulations, the turbulent boundary layer was provided at the inlet with the realistic velocity fluctuations of $Re_\theta = 300$, which were generated using the method of Lund et al. [14]. To ascertain the reliability of the incoming turbulent boundary layer, comparisons of the turbulence statistics with the direct numerical simulation data of Spalart [15] are presented in Fig. 2. Figure 2a shows the profile of the mean velocity normalized by the friction velocity ($U^+ = U/u_\tau$) with variations in $y^+ = yu_\tau/\nu$, and Fig. 2b shows the comparison of the turbulence intensities. The present results are in excellent agreement with those of the previous study. The convective outflow condition $(\partial u_i/\partial t) + U_c(\partial u_i/\partial x) = 0$ is used at the exit, where U_c is the convection velocity. A no-slip boundary condition is imposed at the solid wall. Neumann conditions are imposed at the freestream, and periodic boundary conditions are used in the spanwise direction.

Direct numerical simulations of incompressible flows over an open cavity are performed for $Re_D = 3000$. The cavity flows at high Reynolds number ($Re_D = 12,000$) are simulated using an LES with a dynamic subgrid-scale model [16]. The simulation conditions used in the present study are summarized in Table 1. N_i is the number of grid points in each direction, and the mesh resolutions are nondimensionalized by the friction velocity of the incoming turbulent boundary layer u_τ. The mesh resolutions at the trailing edge and outlet are represented by $\Delta x^+_{\min}$ and $\Delta x^+_{\max}$, respectively. Uniform grids are used in the spanwise direction. Nonuniform grids are used in the streamwise and wall-normal directions, with higher densities of grid points near the leading and trailing edges. As the cavity length is increased, the number of grid points in the streamwise direction is increased to keep the mesh resolution constant. The computational time steps are free from the Courant–Friedrichs–Lewy limit by using the fully implicit decoupling method. The time step is $\Delta t = 0.004D/U_\infty$ for $Re_D = 3000$. For $Re_D = 12,000$, the time step is very small, such as $\Delta t = 0.001875D/U_\infty$, due to the explicit characteristics of the dynamic subgrid-scale model. After a long initial transient period, due to the large residence time of fluid particles in the recirculation zone, the stochastic data are averaged in time as well as in the homogeneous spanwise direction.

The computational domain size is determined after checking two-point correlations of velocity fluctuations. The domain size in the spanwise direction L_Z is 4 times the cavity depth D for $Re_D = 3000$ and 12,000. These spanwise domain sizes are supported by the results of previous numerical simulations of turbulent flows over a backward-facing step [17]. The domain size in the streamwise

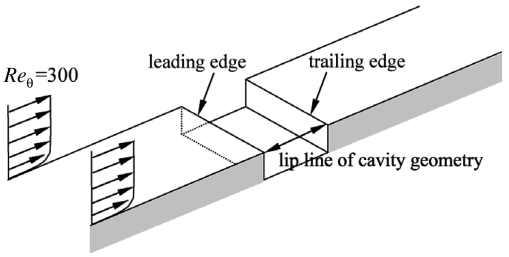

Fig. 1 Schematic diagram of computational domain.

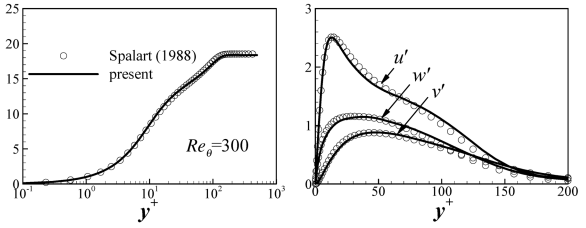

a) U^+ **a) Reynolds stresses**

Fig. 2 Mean velocity and turbulent intensities of turbulent boundary layer, $Re_\theta = 300$.

Table 1 Simulation conditions

Re_D	$L/D, L/\theta$	$N_x \times N_y \times N_z$	$\Delta x^+_{\min}, \Delta x^+_{\max}$	$\Delta y^+_{\min}$	Δz^+	L_z/D
3000	2, 20	$513 \times 133 \times 129$	1.11, 18	0.18	5	4
12,000	2, 80	$897 \times 169 \times 257$	1.4, 40	0.56	10	4

direction is $L_i = L_o = 9D$ for $Re_D = 3000$ and $L_i = 4D$, $L_o = 7.5D$ for $Re_D = 12,000$, respectively. Here, L_i and L_o are the streamwise lengths of the development section before the leading edge and after the trailing edge. The transverse height L_Y is set to be $5D$ for $Re_D = 3000$ and 12,000. The Neumann boundary is imposed at the freestream sufficiently far from the free shear layer of the turbulent cavity flow to allow the turbulent intensity to monotonically decrease to a constant value.

To validate the accuracy of the present simulations, we quantitatively compared the cavity flows of $Re_D = 3000$ in the cavity geometry of $L/D = 2$ with the previous data of Pereira and Sousa [18,19] and Chang et al. [20]. Specifically, we compared the mean streamwise velocity and turbulent intensities at $x/D = 1.4$, that is, the location of the primary vortex core. As shown in Fig. 3, good agreement is observed between the present results and those reported previously. The discrepancy observed in the region of $y/D > 1.4$ is due to differences in the inflow conditions used; that is, we used a fully turbulent boundary layer of $Re_\theta = 300$ in the present simulations, whereas a fully turbulent channel flow of $Re_\theta = 930$ was used in the previous studies. As the turbulent cavity flows of $Re_D = 12,000$ have been compared with PIV data in the previous experiment of Kang et al. [6], the resolution of the present LES is sufficient to analyze the second-order turbulence statistics.

To investigate the oscillating behaviors of a separated shear layer in turbulent flows over an open cavity, we analyzed PIV data obtained from the previous experiment of Kang et al. [6]. The Reynolds number was 25,150 based on the cavity depth of 25 mm and the freestream velocity of $U_\infty = 14$ m/s. The length-to-depth ratio was 2. The Reynolds number of the present experiments is larger than $Re_D = 12,000$ used in the numerical simulations. Because the main emphasis of the present experiments is placed on the successful application of POD analysis to experimental data, the qualitative comparison is reasonably made between the numerical and experimental data. PIV images were acquired using a 12-bit charge-coupled device camera with 1280×1024 pixels. Interrogation windows of 16×16 pixels were used with a 50% overlap. Five-thousand instantaneous PIV images were collected for second-order statistics such as root-mean-square of velocity fluctuations to be stationary. When the instantaneous velocity fields were examined in a reference frame moving at the speed of $0.5U_\infty$, two large-scale vortical structures were observed between the leading and trailing edges. The regular shedding of coherent structures was expected to be responsible for self-sustained oscillations of the separated shear layer. However, it was difficult to investigate the spatial characteristics of coherent structures by examining the instantaneous velocity fields because the quantitative characteristics were dependent on the convection speed of reference frame. For example, the initial formation of coherent structures was obscure in the immediate downstream region of the leading edge because the convection velocity of coherent structures was estimated to be $0.5U_\infty$ on average. To elucidate the spatial characteristics of coherent structures, it is necessary to extract a common pattern of coherent structures by employing the POD analysis to the present experimental data.

III. Proper Orthogonal Decomposition

The classical procedure of POD is based on two-point spatial correlations of stochastic data [21]. The distribution of stochastic data q can be reconstructed in the linear combination of orthogonal basis functions

$$q(\mathbf{x}, t) = \sum_{m=1}^{M} \mu_m \phi_m(t) \psi_m(\mathbf{x}) \tag{3}$$

where ψ_m and ϕ_m is a set of basis functions and time-varying coefficients, respectively. In the linear combination, each basis function is scaled by μ_m. The subscript of m is the sequential number in the dimension M of q. The goal of POD is to seek a set of basis functions to maximize the value of mean square projection, which has the property that the partial sums of Eq. (3) converge faster than the partial sums of any other set of basis functions. Consequently, it amounts to finding a solution of the eigenvalue problem

$$\int_\Omega K(\mathbf{x}, \mathbf{r}) \psi_m(\mathbf{r})\, d\mathbf{r} = \gamma_m \psi_m(\mathbf{x}) \tag{4}$$

where the kernel $K(\mathbf{x}, \mathbf{r})$ is the two-point spatial autocorrelation tensor

$$K(\mathbf{x}, \mathbf{r}) = \langle q(\mathbf{x}) q(\mathbf{x} + \mathbf{r}) \rangle \tag{5}$$

The operator of $\langle \bullet \rangle$ is an averaging of spatial autocorrelation in time. The distribution of q is defined on the physical domain of Ω. The eigenvalue $\gamma_m = \mu_m^2$ represents the energy level of each eigenmode, which is always positive due to the nonnegative definiteness of the kernel function. In a numerical procedure for solving the eigenvalue problem of Eq. (4), the kernel is expressed by a matrix whose size is proportional to a square of physical meshes. For example, the size of a kernel matrix is on the order of billions in the grid system for $Re_D = 12,000$ and $L/D = 2$. Although the eigenmodes can be obtained in the point of theoretical view, it is practically impossible to solve the eigenvalue problem due to its grand size.

An alternative way of building up the kernel is to calculate the covariance of stochastic data based on the concept of temporal correlation [22]. Let us define the kernel as

$$K(\mathbf{x}, \mathbf{r}) := \frac{1}{M} \sum_{i=1}^{M} q^i(\mathbf{x}) q^i(\mathbf{r}) \tag{6}$$

where M is the total number of data. The stochastic data of $q^i(\mathbf{x})$ is defined as the ith image of $q(\mathbf{x}, t)$, that is, $q^i(\mathbf{x}) = q(\mathbf{x}, t_i)$. Sirovich [22] has shown that the problem of Eq. (4) is equivalent to the following eigenvalue problem:

$$\int_\Omega K(\mathbf{x}, \mathbf{r}) \psi_m(\mathbf{r})\, d\mathbf{r} = \gamma_m \psi_m(\mathbf{x}) \tag{7}$$

Assuming a special class of trial function

$$\psi_m(\mathbf{x}) = \sum_{i=1}^{M} c_m^i q^i(\mathbf{x})$$

we obtain

$$\sum_{i=1}^{M} \left[\sum_{j=1}^{M} \left(\frac{1}{M} \int_\Omega q^i(\mathbf{r}) q^j(\mathbf{r})\, d\mathbf{r} \right) c_m^j \right] q^i(\mathbf{x}) = \sum_{i=1}^{M} \gamma_m c_m^i q^i(\mathbf{x}) \tag{8}$$

where i and j are the sequential number of data. It amounts to another eigenvalue problem

$$A \mathbf{c}_m = \gamma_m \mathbf{c}_m \tag{9}$$

where the elements of matrix A is defined as

$$A_{ij} = \frac{1}{M} \int_\Omega q^i(\mathbf{r}) q^j(\mathbf{r})\, d\mathbf{r}$$

and $\mathbf{c}_m = [c_m^1, c_m^2, \ldots, c_m^M]^T$.

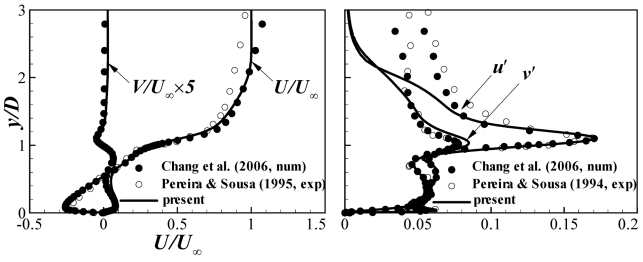

a) b)

Fig. 3 Mean velocities and turbulent intensities of cavity flows when $Re_D = 3000$ ($x/D = 1.4$).

The eigenmodes ψ are calculated from the linear relationship with $\mathbf{c}_m$ as follows:

$$\psi_m(\mathbf{x}) = \sum_{i=1}^{M} c_m^i q^i(\mathbf{x}) \tag{10}$$

If the stochastic data are given by a number of snapshots, the dimension of the kernel matrix is identical to the number of snapshots. Because the snapshot-based POD is designed to identify coherent patterns encountered in snapshots, the basis function of Eq. (10) is strongly dependent on the number of snapshots. To avoid an undesirable dependency, a sufficiently large number of snapshots should be provided to ensure that the statistical properties are stationary. Unfortunately, no systematic test has been carried out in turbulent flows over an open cavity to inform one of how many snapshots are necessary to obtain the convergence of eigenmodes. However, an empirical knowledge suggests that the employment of over 400 snapshots guarantees the independence of dominant eigenmodes on the number of snapshots. To check the dependence of the basis function on the number of snapshots, the convergence of the first eigenmode is shown in Fig. 4 with the concept of residual as follows:

$$\eta(M) = \int_{\Omega} |\psi_1^{M+1}(\mathbf{x}) - \psi_1^{M}(\mathbf{x})|\, d\mathbf{x} \tag{11}$$

where $\psi_1^M(\mathbf{x})$ is the first eigenmode computed by using M snapshots [11]. As seen, the convergence of the first eigenmode is satisfied when the kernel matrix is calculated by using over 400 snapshots.

IV. Proper Orthogonal Decomposition Analysis of Numerical Data

A. $Re_D = 12,000$ & $L/D = 2$

As mentioned earlier, self-sustained oscillations are observed in incompressible turbulent flows over an open cavity when $Re_D = 12,000$ and $L/D = 2$. Over 400 instantaneous snapshots of pressure fluctuations are used for the 2-D POD analysis. In the calculation of the kernel matrix using the instantaneous snapshots, there are two options for choosing the distribution domain of pressure fluctuations. One is to use the entire physical domain including both the upstream region of the leading edge and the downstream region of the trailing edge, as represented in Fig. 5a. Otherwise, to focus on the oscillating behaviors of the separated shear layer, the pressure fluctuations can be considered between the leading and trailing edges, as displayed in Fig. 5b. After comparing two results of POD analyses defined in the full- and subdomain, respectively, it is found that the dominant eigenmodes are essentially the same because most of the pressure fluctuations are produced between the leading and trailing edges. Hereinafter, the POD will be employed to the pressure fluctuations in the subdomain between the leading and trailing edges.

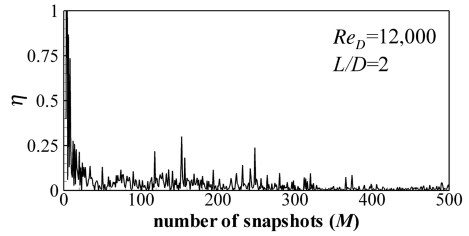

Fig. 4 Convergence of the first eigenmode when $Re_D = 12,000$ and $L/D = 2$.

Figure 6 shows the first six eigenmodes of pressure fluctuations, which are obtained from the 2-D POD analysis. The lip line of cavity geometry is located at $y/D = 1$. The leading and trailing edges are placed at $x/D = 0$ and 2, respectively. One pair of negative and positive distributions represents the low-pressure fluctuations of large-scale vortical structures and the high-pressure fluctuations of induced rotational motions. As seen in the first and second modes, three pairs are clearly observed between the leading and trailing edges. It is consistent with the spectral characteristic of self-sustained oscillations corresponding to $N = 3$, which was reported in Kang et al. [6]. The streamwise length scale of coherent structures gradually increases from $0.3D$ in the immediately downstream region of the leading edge to $0.8D$ in the impingement region near the trailing edge. To avoid any ambiguity, the length-scale of the coherent structure was determined to be twice as long as the streamwise distances between the central locations of positive and negative distributions. The transverse length-scale is not sufficiently large to affect the pressure fluctuations on the bottom wall inside the cavity. It causes the experimental difficulty that the pressure measurement on the bottom wall is not effective for describing self-sustained oscillations of a separated shear layer. The first two modes look like two different phase states of an identical motion, as expected when the flow is experiencing a global mean advection. The phase difference is estimated to be a quarter of one period as if $\sin(x)$ is orthogonal to $\sin(x \pm \pi/2)$. Although the alternative patterns of pressure fluctuations are regularly observed in the first and second

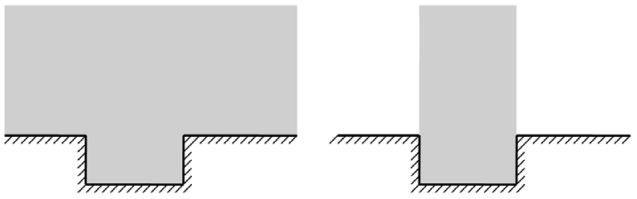

a) Full domain b) Subdomain

Fig. 5 Physical domain for application of POD to pressure fluctuations.

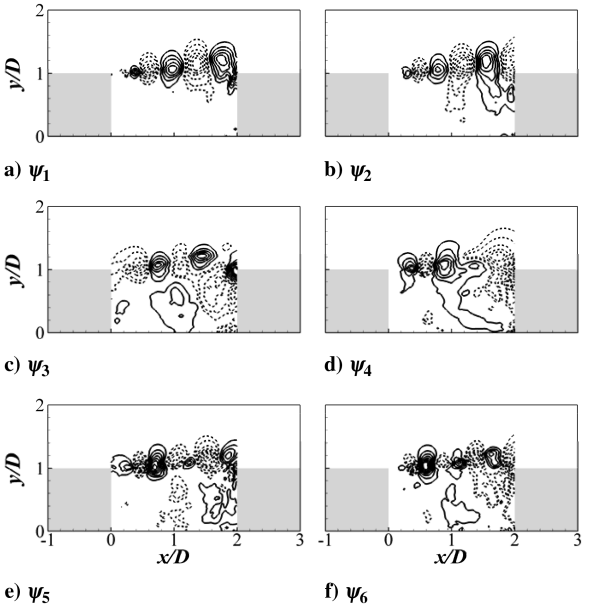

a) ψ_1 b) ψ_2 c) ψ_3 d) ψ_4 e) ψ_5 f) ψ_6

Fig. 6 First six eigenmodes of pressure fluctuations when $Re_D = 12,000$ and $L/D = 2$. The solid and dotted lines represent the positive and negative distributions of eigenmodes.

modes, the distributions are irregular in the third mode of Fig. 6c and the fourth mode of Fig. 6d. The next modes of Figs. 6e and 6f are likely to describe the fluctuating behaviors of a separated shear layer with higher wave numbers, albeit with slight variations. In the previous studies of laminar cavity flows, the oscillating behaviors of a separated shear layer were represented only in the first two modes, whereas the next higher modes were associated with the recirculation of the primary vortex inside the cavity [12]. Simple modes of a separated shear layer produce a single peak frequency in the power spectra of laminar cavity flows. In the present study of turbulent cavity flows, however, the fluctuating behaviors of the separated shear layer are represented in the higher modes as well as in the first two modes. The complex mixture of several modes causes the broad spectra of pressure fluctuations in fluctuating behaviors of a separated shear layer, although the first two modes are responsible for the peak frequency corresponding to $N = 3$.

The contribution of each mode is displayed in Fig. 7a, which is represented by the level of eigenvalues. The square symbols denote the eigenvalues normalized by the total sum of all eigenvalues. The local sum of eigenvalues is represented by the solid line, which is also normalized by the total sum. As shown in Fig. 7a, the contribution of the first two modes is similar, which is approximately 15% of total pressure fluctuations. Close values of γ_1 and γ_2 support that the two modes are originated from identical motions of the separated shear layer. The relationship of the two modes is clearly shown in the phase diagram of Fig. 7b, where the horizontal and vertical axes represent the time-varying coefficients $a_1(t)$ and $a_2(t)$, respectively. The time-varying coefficient $a_m(t)$ of the mth mode is calculated from the following formulation:

$$a_m(t) = \mu_m \phi_m(t) = \int_\Omega p'(\mathbf{x}, t) \cdot \psi_m(\mathbf{x})\, d\mathbf{x} \tag{12}$$

It is interesting to note that a torus is generated by the phase portrait of $a_1(t)$ and $a_2(t)$. Distortion of the circular shape represents the variation of phase difference, whereas dispersion of circulation is caused by the amplitude change of oscillations. If the first two coefficients oscillate with constant amplitude and the phase difference is a quarter of one period, a complete circle is expected to be drawn instead of a torus. The present topological shape of a torus means that small fluctuations of oscillating amplitudes are expected in the first two modes ψ_1 and ψ_2 while the phase difference is nearly constant.

The temporal evolutions of time-varying coefficients are shown in Fig. 8. As seen in Fig. 8a, the periodic signals are observed in the temporal evolutions of $a_1(t)$ and $a_2(t)$. The period of $1.4D/U_\infty$ is exactly consistent with the spectral peak of pressure fluctuations ($\omega = 4.5$) reported in Kang et al. [6]. This means that the spatial modes of ψ_1 and ψ_2 play an important role in the occurrence of self-sustained oscillations. The similarity of phase difference is observed between the spatial modes (ψ_1, ψ_2) and the temporal coefficients (a_1, a_2), that is, the phase difference is approximately a quarter of the spatial wave number and the temporal period. In the higher modes of Figs. 8b and 8c, the fluctuating amplitudes are relatively small compared with those of the first two modes, as expected in the level of eigenvalues. The spectral characteristic is close to nonperiodicity, although the periodic evolutions are intermittently observed in Fig. 8c. From the viewpoint of spatial characteristics, a more instructive view can be derived by examining the temporal evolution of time-varying coefficient $a_1(t)$ in the spanwise direction. Figure 9 shows such time history where the horizontal and vertical axes represent the spanwise direction and time, respectively. The time-varying coefficient is similarly distributed in the spanwise direction. For example, the positive coefficients of Fig. 9 are overall distributed in the spanwise direction at $tU_\infty/D = 0, 2, 4$, whereas the spanwise distributions of negative coefficients are observed at $tU_\infty/D = 1, 3, 5$. Considering that the streamwise length scales of coherent structures are only $0.3 \sim 0.8D$, the first mode is quasi-two-dimensional in the spanwise direction even though it is not fully 2-D due to a little variation. It can also be expected for the second mode to be quasi-two-dimensional.

Now, it is useful to propose a simple procedure to estimate the qualitative velocity field corresponding to each POD mode of pressure fluctuations. As known, multipoint linear stochastic estimation (mLSE) can be a good candidate to guess a vector field of velocity fluctuations corresponding to a scalar distribution of pressure fluctuations [10,23]. In the present study, however, a large number of instantaneous pressure fluctuations fields were provided instead of spatial correlations. The usage of conditional averaging is more convenient than mLSE if an appropriate condition is given in the distribution of pressure fluctuations. In the calculation of the time-varying coefficients $a_m(t)$ by using Eq. (12), the coefficient can be regarded as an instantaneous correlation coefficient between the instantaneous pressure fluctuations $p'(\mathbf{x}, t)$ and the mth eigenmode

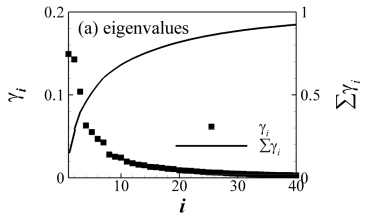

a) Eigenvalues

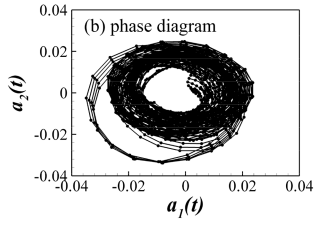

b) Phase diagram

Fig. 7 Relationship of eigenmodes: a) level of eigenvalues and b) phase diagram of time-varying coefficients $a_1(t)$ and $a_2(t)$ when $Re_D = 12,000$.

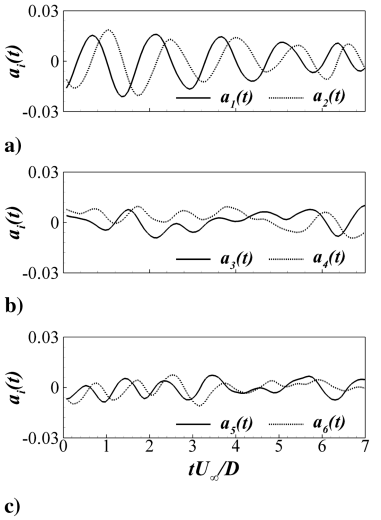

Fig. 8 Temporal evolution of time-varying coefficients when $Re_D = 12,000$.

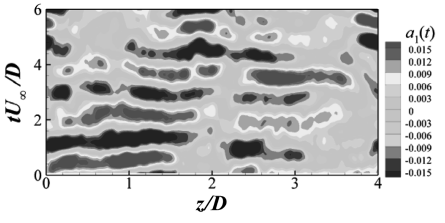

Fig. 9 Spanwise distributions of time-varying coefficients $a_1(t)$ when $Re_D = 12,000$.

$\psi_m(\mathbf{x})$. If $a_m(t)$ is very large in an instantaneous distribution of pressure fluctuations, it means that the instantaneous distribution is very similar to the mth eigenmode. When the instantaneous velocity fluctuations fields are conditionally averaged under the criterion of sufficiently strong correlation, as follows,

$$\langle u' | a_m(t) \geq \alpha_m \rangle = \underline{u}'_m(\mathbf{x}) \tag{13}$$

we can qualitatively estimate the velocity fluctuations field $\underline{u}'_m(\mathbf{x})$ corresponding to the mode $\psi_m(\mathbf{x})$ of pressure fluctuations. The underline operator '' represents a conditional averaging. If the pressure fluctuations are measured at one point ($x = x_0$), the basis function is defined as a delta function, $\delta(\mathbf{x} - x_0)$. The mathematical formulation of conditional averaging is derived as

$$\langle u' | p'(x_0, t) \geq \alpha_1 \rangle = \underline{u}'(\mathbf{x}) \quad \text{if } \psi_1(\mathbf{x}) = \delta(\mathbf{x} - x_0) \tag{14}$$

This means that the conditional averaging is carried out when the pressure fluctuations at the point are larger than a threshold. Consequently, the concept of Eq. (13) is identical to the conditional averaging which has been generally used in the turbulent flows over a backward-facing step [24,25].

The conditional averaging is carried out under the criterion of Eq. (13). Figure 10 shows the distributions of velocity fluctuations corresponding to the first two modes of pressure fluctuations. The threshold is set to be $\alpha_m = 2(a_m)_{\text{rms}}$. Several values of the threshold have been tested but the velocity distribution was found to be almost the same when the threshold was larger than 1.5. The velocity fluctuations are consistent with the distributions of pressure fluctuations, as seen in Fig. 10. In Figs. 10a and 10c, the positive distributions and the counterclockwise rotations are concurrently observed at $x/D = 0.4$, 0.9, and 1.8, whereas the negative distributions and the clockwise rotations coexist at $x/D = 0.2$, 0.6, and 1.3. The negative pressure fluctuations are generated by large-scale vortical structures with the clockwise rotation, whereas the induced counterclockwise rotations are responsible for the positive pressure fluctuations. In Figs. 10b and 10d, we can observe the negative distributions of pressure fluctuations with the counterclockwise rotations near $x/D = 0.5$ and 1.2. The third vortical structure is going to be ejected from the cavity near $x/D = 2.0$. This consistency shows a successful estimation of velocity fields corresponding to the dominant eigenmodes.

B. $Re_D = 3000$ & $L/D = 2$

When $Re_D = 3000$ and $L/D = 2$, no oscillations are observed in incompressible turbulent flows over an open cavity. The same POD analysis is carried out by using over 400 snapshots of instantaneous pressure fluctuations. The first six modes are shown in Fig. 11. The solid and dotted lines represent the positive and negative distributions of eigenmodes, respectively. As seen in Figs. 11a and 11b, it is hard to assert that two complete pairs of positive and negative distributions are observed between the leading and trailing edges. The number of pairs is closer to 1.5, rather than 2. Assuming that the convection velocity is similar to $0.49U_\infty$ of $Re_D = 12,000$, the peak frequency ($\omega = 2.3$) of pressure fluctuations corresponds to $N = fL/U_C = 1.49$. The first and second modes are responsible for the spectral peak of pressure fluctuations. Because both the number of structural pairs and the spectral modes N are not integers, the fluctuating behaviors of the separated shear layer is not originated from a geometric peculiarity of the cavity [26]. With the exception of the sixth mode, other higher modes are likely to describe the fluctuating behaviors of the separated shear layer with higher wave numbers, as seen in Figs. 11c–11e.

The observation of eigenvalues provides the modal contribution to pressure fluctuations in Fig. 12a. Although the first and second eigenvalues are very dominant with the levels of 21 and 20%, respectively, other eigenvalues are insignificant, especially for

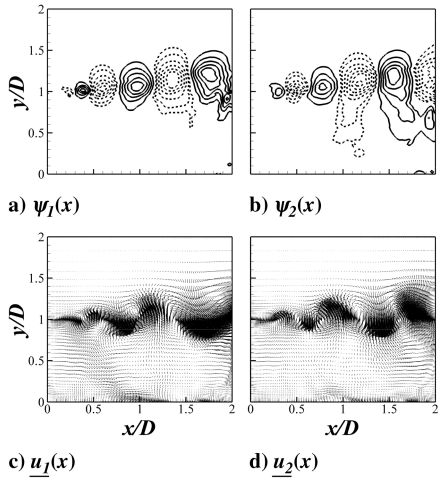

Fig. 10 Estimation of velocity field corresponding to each eigenmode of pressure fluctuations based on the concept of conditional averaging when $Re_D = 12,000$ and $L/D = 2$. The solid and dotted lines represent the positive and negative distributions of eigenmodes.

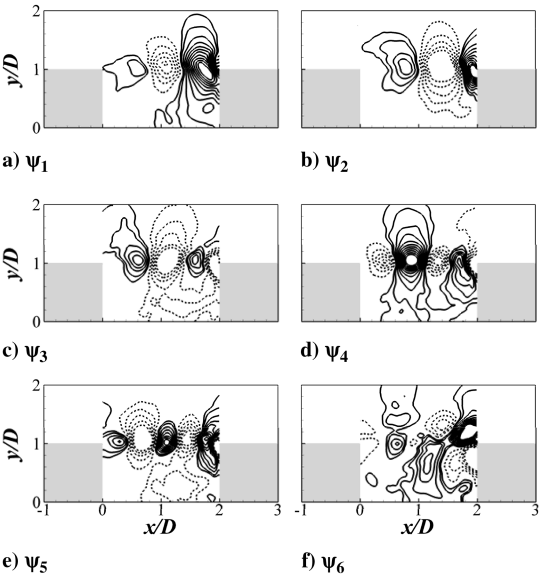

Fig. 11 First six eigenmodes of pressure fluctuations when $Re_D = 3000$ and $L/D = 2$. The solid and dotted lines represent the positive and negative distributions of eigenmodes.

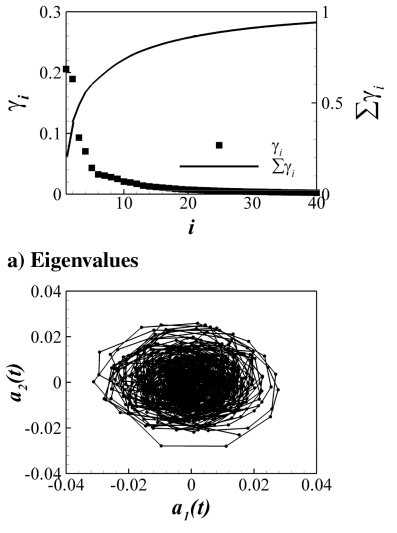

Fig. 12 Relationship of eigenmodes: a) the level of eigenvalues and b) phase diagram of time-varying coefficients $a_1(t)$ and $a_2(t)$ when $Re_D = 3000$.

modes higher than the fifth mode. Because the first two modes look very similar and their eigenvalues are closely dominant, the two modes can be expected to arise from an identical motion of the separated shear layer, likewise for $Re_D = 12,000$. The phase trace of two coefficients $a_1(t)$ and $a_2(t)$ is displayed in Fig. 12b. The distribution of the phase portrait cannot be explained by random differences of phase. The phase relationship is portrayed by the overall counterclockwise circulation, although both dispersion and distortion are observed. To elucidate the temporal characteristic of each mode in detail, the time-varying coefficient $a_i(t)$ of the ith mode is shown in Fig. 13. The temporal variations of the first two coefficients are large, whereas other coefficients are sufficiently small as expected in the levels of eigenvalues. As shown in Fig. 13a, considerable fluctuations are observed in the amplitudes of $a_1(t)$ and $a_2(t)$. Based on the temporal correlation, however, the lag time between two coefficients is almost constant at $\Delta t = 0.65D/U_\infty$, which is consistent with a quarter of one period ($\omega = 2.3$). Why do the amplitudes of $a_1(t)$ and $a_2(t)$ significantly fluctuate in Fig. 13a despite of the constant lag time? The answer is placed on the three-dimensionality of the fluctuating behaviors, which are represented by the first two modes ψ_1 and ψ_2. The temporal evolution of the time-varying coefficient $a_1(t)$ is examined in the spanwise direction to investigate the three-dimensionality of the first mode. In Fig. 14a, the horizontal and vertical axes represent the spanwise direction and time, respectively. The spatial variation of coefficient magnitude suggests the three-dimensionality of the first mode ψ_1. To make it clear, the spanwise distributions of the first coefficient are

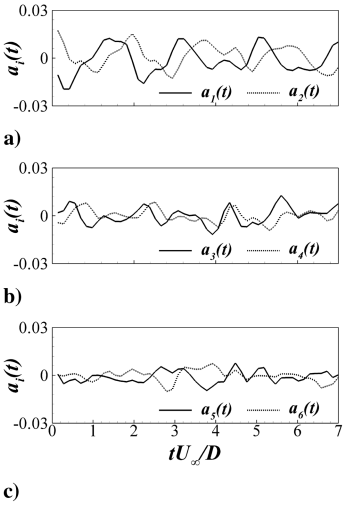

Fig. 13 Temporal evolution of time-varying coefficients when $Re_D = 3000$.

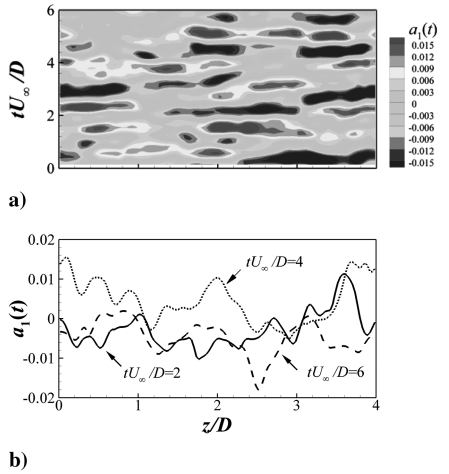

Fig. 14 Spanwise distributions of time-varying coefficients $a_1(t)$ when $Re_D = 3000$.

demonstrated in Fig. 14b at three instants. The solid, dotted, and dashed lines represent the spatial distributions of $a_1(t)$ at $tU_\infty/D = 2$, 4, and 6, respectively. As seen, the coherent structures represented by the first mode ψ_1 are fully 3-D. The spatial three-dimensionality inevitably causes the temporal fluctuations of the coefficient amplitude in the 2-D POD due to the loss of dimension. Even if the three-dimesional POD is carried out, there is little possibility that a periodic signal of $a_1(t)$ can be obtained without any fluctuations of amplitude. Because the spanwise characteristics of ψ_1 are irregular in location, length scale, and swirling strength of the coherent structures, it will be difficult to provide a representative 3-D pattern of pressure fluctuations. Consequently, the spatial three-dimensionality and the temporal fluctuations are the essential properties of coherent structures, which are presented in turbulent cavity flows for $Re_D = 3000$ and $L/D = 2$.

V. Proper Orthogonal Decomposition Analysis of Experimental Data

Before now, the spatial structures responsible for self-sustained oscillations were successfully disclosed by employing the snapshot-based POD to the 2-D distributions of pressure fluctuations. Although the distribution of pressure fluctuations is a good measurement to identify large-scale coherent structures, it is not a practical variable in experiments. An available variable should be suggested for the application of POD to experimental data such as PIV images and hot-wire signals. The fluctuating behaviors of the separated shear layer are well demonstrated in the statistical analyses of transverse velocity fluctuations, as reported in previous experimental results. Ashcroft and Zhang [5] have reported that the alternative patterns of positive and negative v-v correlation coefficients represent the organized nature of coherent structures. The alternative patterns have been also observed in the v-v correlations of Kang et al. [6], as well as Ukeiley and Murray [27]. Chatellier et al. [28] used the linear distributions of transverse velocity to describe the unsteady motions of a separated shear layer as well.

Based on the previous reports, the transverse velocity fluctuations are chosen to be used in the application of POD analysis to experimental data. To check the effectiveness of transverse velocity fluctuations, the classic procedure of POD is employed to the numerical data of turbulent flows over an open cavity when $Re_D = 12,000$ and $L/D = 2$. The distribution of v-v correlations are defined on the lip line of cavity geometry to exclude irrelevant fluctuations of transverse velocity to the oscillating behaviors of the separated shear layer. The transverse velocity fluctuations can be expressed by the linear combination of a set of basis functions as follows:

$$v(x,t) = \sum_{m=1}^{M} \mu_m \phi_m(t) \sigma_m(x) \tag{15}$$

where $\sigma_m(x)$ represents the mth eigenmode. Figure 15a shows the first two eigenmodes σ_1 and σ_2, which represent oscillating behavior of the separated shear layer. As shown, the initial formation of coherent structures looks vague in the immediate downstream region of the leading edge, and the oscillation is significantly disturbed near the trailing edge due to the impingement of vortical structures. Nevertheless, three vortical structures are organized between the leading and trailing edges. Figures 15b and 15c represent the correspondent distributions of pressure fluctuations, which are conditionally averaged as mentioned earlier. The solid and dotted lines denote the positive and negative pressure fluctuations, respectively. The overall distribution of pressure fluctuations is very similar to the first and second eigenmodes of Fig. 6, although small discrepancies are observed in the streamwise locations of positive and negative distributions. Because the negative pressure fluctuations represent the vortical formation of coherent structures, three vortical structures are clearly observed between the leading and trailing edges. The length scale of coherent structures gradually increases from $0.3D$ in the immediate downstream region of the

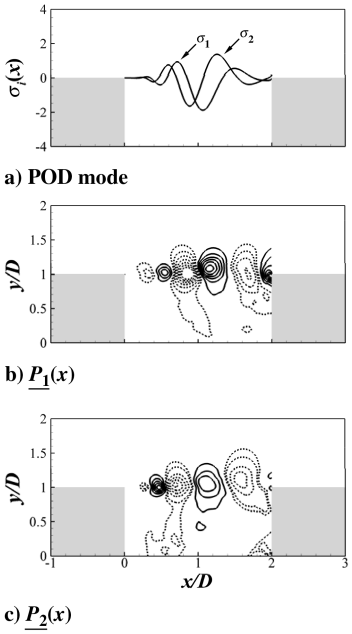

Fig. 15 POD analysis of transverse velocity fluctuations when $Re_D = 12,000$ and $L/D = 2$: a) first two eigenmodes of transverse velocity fluctuations on the lip line of cavity geometry, b) spatial distributions of pressure fluctuations corresponding to σ_1, and c) corresponding to σ_2. The solid and dotted lines represent the positive and negative distributions of eigenmodes.

leading edge to $0.8D$ in the impingement region near the trailing edge.

By the same procedure, the spatial correlations of transverse velocity fluctuations are calculated from PIV data of Kang et al. [6]. After the POD analysis is employed to the spatial distributions of v-v correlations on the lip line of cavity geometry, the eigenmodes of transverse velocity fluctuations are obtained as shown in Fig. 16a. The first two eigenmodes are related to the oscillating behavior of the separated shear layer, in which two vortical structures are observed between the leading and trailing edges. To elucidate the spatial formation of coherent structures in detail, instantaneous velocity fields are conditionally averaged based on the eigenmodes.

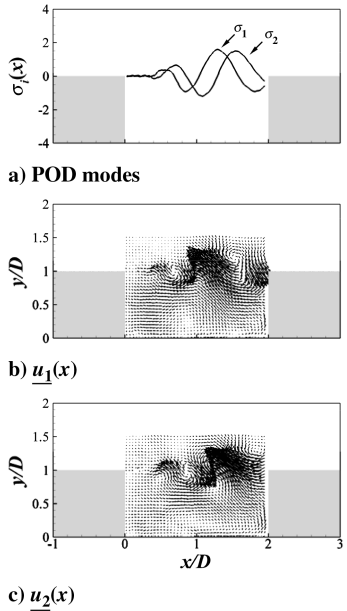

Fig. 16 Experimental application of POD analysis: a) first two eigenmodes of transverse velocity fluctuations on the lip line of cavity geometry, b) spatial distributions of pressure fluctuations corresponding to σ_1, and c) corresponding to σ_2.

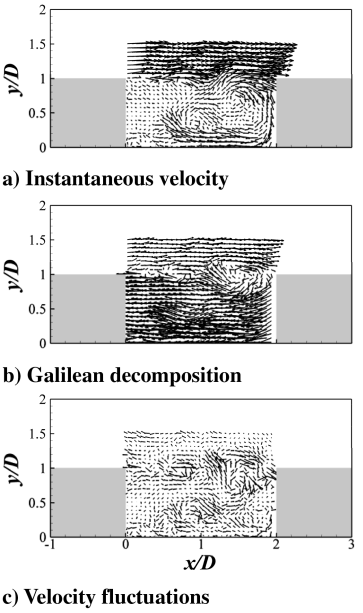

Fig. 17 Instantaneous evidence of large-scale vortical structures: a) instantaneous distributions of velocity field, b) Galilean decomposed distributions of velocity field, and c) instantaneous distributions of velocity fluctuations.

Figures 16b and 16c show the conditional-averaged distributions of velocity fluctuations corresponding to the first two eigenmodes, respectively. In the first mode of Fig. 16b, the large-scale vortical structures are observed near $x/D = 0.7$ and 1.5. In the second mode of Fig. 16c, one vortical structure is shed downstream near $x/D = 0.9$ and the other is likely to be ejected from the cavity near $x/D = 1.8$. It is clear that two vortical structures are responsible for self-sustained oscillations of the separated shear layer. As expected, the patterns of Figs. 16b and 16c are frequently encountered in the majority of instantaneous velocity fields. Figure 17a shows a representative velocity field when the time-varying coefficient of the first eigenmode is large. When Galilean decomposition is employed to the velocity field with the convection velocity of $0.5U_\infty$, the two vortical structures are qualitatively identified in Fig. 17b. The streamwise location and length scale of vortical structures are consistent with the velocity distributions of Fig. 16a. However, the vortical formation of large-scale structures is obscure in the vector fields of velocity fluctuations, as shown in Fig. 17c, although the vortical formations could be guessed from the enhancement of velocity fluctuations. From the viewpoint of statistical analysis in experiments, the POD analysis is very effective to extract large-scale vortical structures in turbulent flow over an open cavity when the analysis is employed to the spatial distributions of v-v correlations on the lip line of cavity geometry.

VI. Conclusions

In the present study, we identified large-scale vortical structures responsible for self-sustained oscillations by employing proper orthogonal decompositions to pressure fluctuations of turbulent flows over an open cavity. To reduce the dimension of the eigenvalue problem, the snapshot-based POD was applied to the distributions of pressure fluctuations. The residual of the first eigenmode showed the satisfaction of convergence when the kernel matrix was calculated by using over 400 snapshots. When self-sustained oscillations took place for $Re_D = 12,000$ and $L/D = 2$, three pairs of alternative patterns were observed in the first and second modes of pressure fluctuations. This was consistent with spectral characteristics of self-sustained oscillations corresponding to $N = 3$. By examining the phase diagram of time-varying coefficients and the level of eigenvalues, the first two eigenmodes were found to represent two different phase states of an identical self-sustained oscillation. Both temporal evolution and spanwise distribution of the first two modes

disclosed that quasi-two-dimensional formation of large-scale vortical structures gives rise to self-sustained oscillations of a separated shear layer. However, three-dimensional vortical structures were identified in the dominant modes of pressure fluctuations when the oscillations were not observed for $Re_D = 3000$ and $L/D = 2$. Because the spatial characteristics of dominant eigenmodes were irregular in location, length scale, and swirling strength of coherent structures, the spatial three-dimensionality was an essential property of coherent structures that were presented in turbulent cavity flows for $Re_D = 3000$. Although the large-scale coherent structures were successfully identified in the POD of pressure fluctuations, the availability could not be extended to experimental data. For the application of POD analysis to experimental data, the decomposition was employed to the spatial distributions of v-v correlations on the lip line of cavity geometry. After obtaining the first two eigenmodes representing the oscillating behaviors of the separated shear layer, instantaneous velocity fields were conditionally averaged under the criterion of a strong correlation between the instantaneous distributions of transverse velocity fluctuations and the first two eigenmodes. In the conditional-averaged distributions of velocity fluctuations, the large-scale vortical structures responsible for self-sustained oscillations were clearly identified. The vortical formations of coherent structures were frequently encountered in the majority of instantaneous velocity fields, as disclosed by Galilean decomposition of an instantaneous velocity field.

References

[1] Rossiter, J. E., "Wind-Tunnel Experiments on the Flow over Rectangular Cavities at Subsonic and Transonic Speeds," Aeronautical Research Council Rept. and Memoranda, No. 3438, 1964.

[2] Ahuja, K., and Mendosa, J., "Effects of Cavity Dimensions, Boundary Layer and Temperature on Cavity Noise with Emphasis on Benchmark Data to Validate Computational Aeroacoustics Codes," Final Rept. Contract NASA-19061, Task 13. NASA Contract Rept., 1995.

[3] Rowley, C. W., Colonius, T., and Basu, A. J., "On Self-Sustained Oscillations in Two-Dimensional Compressible Flow over Rectangular Cavities," *Journal of Fluid Mechanics*, Vol. 455, 2002, pp. 315–346. doi:10.1017/S0022112001007534

[4] Lin, J.-C., and Rockwell, D., "Organized Oscillations of Initially Turbulent Flow Past a Cavity," *AIAA Journal*, Vol. 39, No. 6, 2001, pp. 1139–1151.

[5] Ashcroft, C., and Zhang, X., "Vortical Structures over Rectangular Cavities at Low Speed," *Physics of Fluids*, Vol. 17, No. 1, 2005, p. 015104. doi:10.1063/1.1833412

[6] Kang, W., Lee, S. B., and Sung, H. J., "Self-Sustained Oscillations of Turbulent Flows over an Open Cavity," *Experiments in Fluids* [published online], 30 April 2008. doi:10.1007/s00348-008-0510-8

[7] Lumley, J. L., "The Structure of Inhomogeneous Turbulence," *Atmosphere Turbulence and Wave Propagation*, edited by A. M. Yaglom, and V. I. Tatarsky, Nauka, Moscow, 1967, p. 166.

[8] Liu, Z., Adrian, R. J., and Hanratty, T. J., "Large-Scale Modes of Turbulent Channel Flow: Transport and Structure," *Journal of Fluid Mechanics*, Vol. 448, 2001, pp. 53–80.

[9] Kostas, J., Soria, J., and Chong, M. S., "Particle Image Velocimetry Measurements of a Backward-Facing Step," *Experiments in Fluids*, Vol. 33, 2002, pp. 838–853.

[10] Hudy, L. M., Naguib, A., and Humphreys, L. M., "Stochastic Estimation of a Separated-Flow Field Using Wall-Pressure-Array Measurements," *Physics of Fluids*, Vol. 19, No. 2, 2007, p. 024103. doi:10.1063/1.2472507

[11] Pastur, L. R., Lusseyran, F., Fraigneau, Y., and Podvin, B., "Determining the Spectral Signature of Spatial Coherent Structures in an Open Cavity Flow," *Physical Review E (Statistical Physics, Plasmas, Fluids, and Related Interdisciplinary Topics)*, Vol. 72, Dec. 2005, p. 065301(R). doi:10.1103/PhysRevE.72.065301

[12] Podvin, B., Fraigneau, Y., Lusseyran, F., and Gougat, P., "A Reconstruction Method for the Flow Past an Open Cavity," *Journal of Fluids Engineering*, Vol. 128, No. 3, 2006, pp. 531–540. doi:10.1115/1.2175159

[13] Kim, K., Baek, S.-J., and Sung, H. J., "An Implicit Decoupling Procedure for the Incompressible Navier–Stokes Equations," *International Journal for Numerical Methods in Fluids*, Vol. 38, No. 2, 2002, pp. 125–138. doi:10.1002/fld.205

[14] Lund, T. S., Wu, X., and Squires, K. D., "Generation of Turbulent Inflow Data for Spatially-Developing Boundary Layer Simulation," *Journal of Computational Physics*, Vol. 140, No. 2, 1998, pp. 233–258. doi:10.1006/jcph.1998.5882

[15] Spalart, P. R., "Direct Simulation of a Turbulent Boundary Layer up to $Re_\theta = 1410$," *Journal of Fluid Mechanics*, Vol. 187, 1988, pp. 61–98. doi:10.1017/S0022112088000345

[16] Germano, M., Piomelli, U., Moin, P., and Cabot, W. H., "A Dynamic Subgrid-Scale Eddy Viscosity Model," *Physics of Fluids*, Vol. 3, No. 7, 1991, pp. 1760–1765. doi:10.1063/1.857955

[17] Le, H., Moin, P., and Kim, J., "Direct Numerical Simulation of Turbulent Flow over a Backward-Facing Step," *Journal of Fluid Mechanics*, Vol. 330, 1997, pp. 349–374. doi:10.1017/S0022112096003941

[18] Pereira, J. C. F., and Sousa, J. M. M., "Influence of Impingement Edge Geometry on Cavity Flow Oscillations," *AIAA Journal*, Vol. 32, No. 8, 1994, pp. 1737–1740. doi:10.2514/3.12168

[19] Pereira, J. C. F., and Sousa, J. M. M., "Experimental and Numerical Investigation of Flow Oscillations in a Rectangular Cavity," *Journal of Fluids Engineering*, Vol. 117, No. 1, 1995, pp. 68–74. doi:10.1115/1.2816825

[20] Chang, K. C., Constantinescu, G., and Park, S.-O., "Analysis of the Flow and Mass Transfer Processes for the Incompressible Flow Past an Open Cavity with a Laminar and a Fully Turbulent Incoming Boundary Layer," *Journal of Fluid Mechanics*, Vol. 561, 2006, pp. 113–145. doi:10.1017/S0022112006000735

[21] Berkooz, G., Holmes, P., and Lumley, J. L., "The Proper Orthogonal Decomposition in the Analysis of Turbulent Flows," *Annual Review of Fluid Mechanics*, Vol. 25, Jan. 1993, pp. 539–575. doi:10.1146/annurev.fl.25.010193.002543

[22] Sirovich, L., "Turbulence and the Dynamics of Coherent Structures," *Quarterly of Applied Mathematics*, Vol. 45, No. 3, 1987, pp. 561–590.

[23] Murray, N. E., and Ukeiley, L. S., "Estimation of the Flow Field from Surface Pressure Measurements in an Open Cavity," *AIAA Journal*, Vol. 41, No. 5, 2003, pp. 969–972. doi:10.2514/2.2035

[24] Lee, I., and Sung, H. J., "Multiple-Arrayed Pressure Measurement for Investigation of the Unsteady Flow Structure of a Reattaching Shear Layer," *Journal of Fluid Mechanics*, Vol. 463, 2002, pp. 377–402.

[25] Kiya, M., and Sasaki, K., "Structure of Large-Scale Vortices and Unsteady Reverse Flow in the Reattaching Zone of a Turbulent Separation Bubble," *Journal of Fluid Mechanics*, Vol. 154, 1985, pp. 463–491. doi:10.1017/S0022112085001628

[26] Gharib, M., and Roshko, A., "The Effect of Flow Oscillations on Cavity Drag," *Journal of Fluid Mechanics*, Vol. 177, 1987, pp. 501–530. doi:10.1017/S002211208700106X

[27] Ukeiley, L., and Murray, N. E., "Velocity and Surface Measurements in an Open Cavity," *Experiments in Fluids*, Vol. 38, No. 5, 2005, pp. 656–671. doi:10.1007/s00348-005-0948-x

[28] Chatellier, L., Laumonier, Y., and Gervais, Y., "Theoretical and Experimental Investigations of Low Mach Number Turbulent Cavity Flows," *Experiments in Fluids*, Vol. 36, No. 5, 2004, pp. 728–740. doi:10.1007/s00348-003-0752-4

P. Givi
Associate Editor